Available online at www.sciencedirect.com
SCIENCE DIRECT
Lithos 90 (2006) 43–56
LITHOS
www.elsevier.com/locate/lithos

Harzburgite–dunite–orthopyroxenite suite as a record of supra-subduction zone setting for the Oman ophiolite mantle

Akihiro Tamura *, Shoji Arai

Department of Earth Sciences, Kanazawa University, Kakuma, Kanazawa 920-01192, Japan

Received 7 April 2005; accepted 27 December 2005
Available online 10 March 2006

Abstract

We found a harzburgite–dunite–orthopyroxenite suite from the West Jizi block in the northern Oman ophiolite as a record of supra-subduction zone magmatism in the mantle. The orthopyroxenite has features of parallel dikes, each dike being 10–30 cm thick and in direct contact with the host harzburgite. The orthopyroxenite is composed of orthopyroxene (>95 vol.%), clinopyroxene (<5 vol.%) and trace spinel (<1 vol.%), and is free from olivine. All rocks from the suite are characterized by high Cr# [=Cr/(Cr+Al) atomic ratio] of spinel (Cr#≥0.65). The Fo content of olivine is relatively low, 89.9 to 91.1, in harzburgite and dunite. Clinopyroxenes are very low in incompatible elements and show LREE enrichment in orthopyroxenite and host harzburgite. Similar trace element concentrations of clinopyroxenes in the harzburgite and orthopyroxenite suggest their genetic linkage: the harzburgite is a residue of a partial melting, and its extracted melt formed orthopyroxenite dike. The melt in equilibrium with clinopyroxene is similar in trace-element characteristics to boninite. The mineral chemistries indicate that the harzburgite experienced higher degree of partial melting than abyssal peridotite. LREE-enriched melt and/or fluid assisted the high-degree melting. These lines of evidence indicate an involvement of arc magma in the rock suite genesis, i.e. a supra-subduction zone setting experienced by the Oman ophiolite mantle.

Keywords: Depleted harzburgite; Orthopyroxenite; High-Cr# spinel; Oman ophiolite; Arc-related mantle; Boninite magma

1. Introduction

The Oman ophiolite is regarded as a fragment of Cretaceous oceanic lithosphere, composed of oceanic crust and upper mantle. The well-preserved ophiolitic sequence provides best outcrops to investigate the magmatic and tectonic processes concerning with the oceanic lithosphere formation at a spreading center. The formation of the Oman ophiolite, however, is still controversial in terms of the tectonic setting; mid-ocean ridge origin (e.g., Nicolas, 1989) or supra-subduction zone origin (e.g., Alabaster et al., 1982; Lippard et al., 1986). The latter has been proposed by materials from the crustal sequence, for example, LIL element-enriched lavas indicating arc-related magmatism (e.g. Alabaster et al., 1982). Ishikawa et al. (2002) reported boninitic lavas and dikes from the northern Oman ophiolite, and suggested that they were formed in an early stage of the subduction zone setting. On the other hand, the critical material indicating supra-subduction zone setting has not been discovered from the mantle sequence. The mantle sequence of the Oman

* Corresponding author.
E-mail address: kamui@kenroku.kanazawa-u.ac.jp (A. Tamura).

0024-4937/$ - see front matter © 2006 Elsevier B.V. All rights reserved.
doi:10.1016/j.lithos.2005.12.012

ophiolite is of harzburgite-type (Nicolas, 1989) although lherzolite has been reported from the basal section of the mantle sequence (Lippard et al., 1986; Godard et al., 2000; Takazawa et al., 2003). The harzburgite and lherzolite are similar in petrological features, for example, limited Cr# [=Cr/(Cr+Al) atomic ratio] of spinel (Cr#<0.6), to residual peridotite from the fast spreading mid-ocean ridges (e.g. Kelemen et al., 1995). However, harzburgites with higher-Cr# (>0.65) spinel were rarely found from the mantle sequence of several areas (Matsukage et al., 2001; Le Mée et al., 2004) and, recently, Kanke and Takazawa (2005) revealed spatial distribution of such a harzburgite in the northern area (northern Fizh block). Dunite also contains high-Cr# spinel, which was explained by the reaction between mantle and mid-ocean ridge basalt (MORB) magma (Kelemen et al., 1995). Harzburgite with such a high-Cr# spinel has been reported from the mantle sequences in other ophiolites (e.g. Batanova and Sobolev, 2000; Suhr and Edwards, 2000). In the Bay of Islands ophiolite, for example, Suhr and Edwards (2000) proposed that the harzburgite was formed by remelting under the supra-subduction zone setting. Pyroxenite dykes within the harzburgite have also been well studied and they are considered products formed by arc-related magmatism (Edwards, 1995; Varfalvy et al., 1996, 1997). Pyroxenite veins or layers are common members in the mantle sequence of the Oman ophiolite and their classification and origin have been examined by Gregory (1984) and Python and Ceuleneer (2003). According to Python and Ceuleneer (2003), orthopyroxenites are quite rare relative to other types of pyroxenite (e.g., clinopyroxenite or websterite) through the mantle sequence, and they proposed that the all pyroxenites were formed by magmatism at a mid-ocean ridge setting. In this paper, we report a harzburgite–dunite–orthopyroxenite suite in the mantle sequence of the Oman ophiolite. The main purpose of this study is to report the petrological data of the residual peridotite with high-Cr# spinel from the Oman ophiolite. Then we propose that the suite genetically corresponds to arc-related mantle and discuss that the Oman ophiolite mantle recorded supra-subduction zone setting.

2. Geologic background

The Oman ophiolite is a fragment of the Tethyan oceanic lithosphere obducted onto the Arabian continent. It forms the Oman Mountains running parallel to the coastline of the Sultanate of Oman (Fig. 1a). The

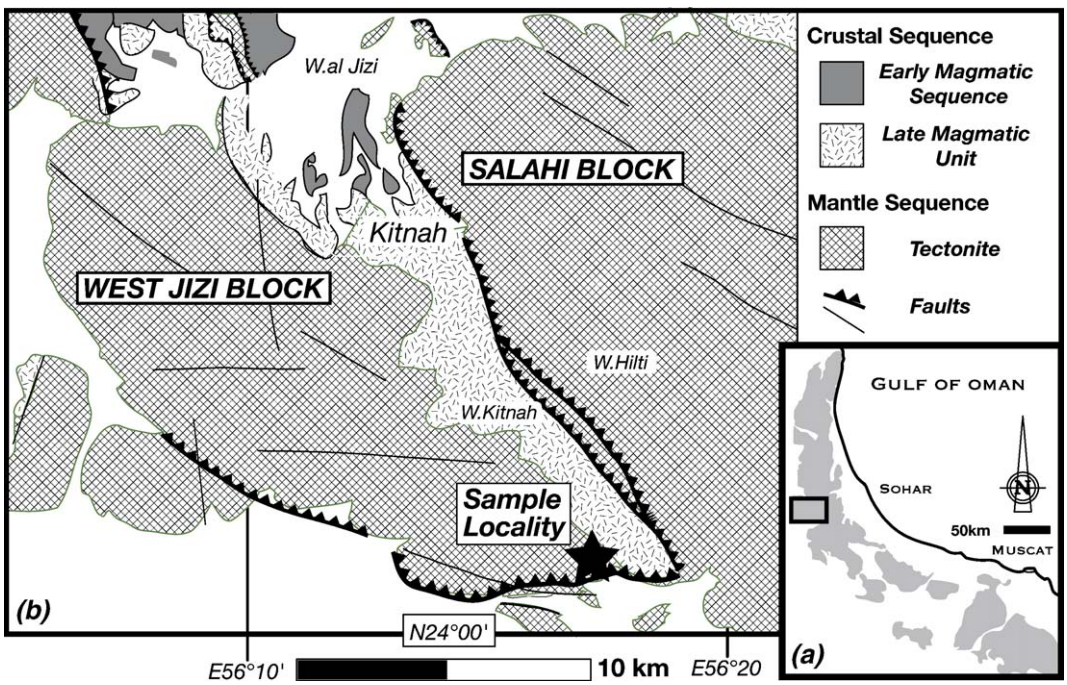

Fig. 1. (a) Distribution of the Oman ophiolite (gray) (after Lippard et al., 1986) with study area (square). (b) Geological map of the West Jizi block and the locality of the harzburgite–dunite–orthopyroxenite suite (sample locality). Simplified from 1:250,000 geological map of Buraymi (Le Métour et al., 1992).

ophiolite extends to NW–SE direction exceeding 600 km in length and 75–130 km in width. The Oman ophiolite consists of 12 tectonic blocks formed by syn- and post-emplacement faulting and folding (Lippard et al., 1986). Each block has well preserved original internal stratigraphy of the ophiolite composed of mantle sequence (8–12 km in thickness) and crustal sequence (4–9 km in thickness). The crustal sequence is composed of, from base to top, layered peridotite and gabbro, non-layered plutonic rocks, sheeted dike complex and extrusive sequence of lavas interbedded with and overlain by pelagic and metalliferous sediments (Lippard et al., 1986). The mantle sequence mainly comprises harzburgite and dunite with dikes of gabbros and pyroxenites (e.g., Lippard et al., 1986; Nicolas, 1989). Lherzolite is distributed along the basal part of the mantle sequence in some blocks (Godard et al., 2000; Takazawa et al., 2003). The base of the block consists of up to 500 m of mylonitized peridotites (Banded Unit), which is underlain by a meta-sediment unit (metamorphic sole) (Lippard et al., 1986). The deformation and metamorphism were undergone during emplacement of the ophiolite block. Radiometric dating of pelagiogranite and dating of radiolarian fauna from the pelagic sediments indicate that the crustal sequence of the Oman ophiolite has mid-Cretaceous ages (about 95 Ma) (Tilton et al., 1981).

3. Locality and sample descriptions

Studied samples were collected from a harzburgite–dunite–orthopyroxenite suite in the southern part of the West Jizi block (Fig. 1). According to the geological maps of Lippard et al. (1986) and Le Métour et al. (1992), the northern part of the West Jizi block has a complete ophiolite sequence, but the mantle section and late intrusive rocks are directly thrusted over by the mantle sequence of the Salahi block in the southern part. Southern West Jizi block is composed of the mantle peridotite and late intrusives with the banded unit and basal serpentinite mélange (Lippard et al.,

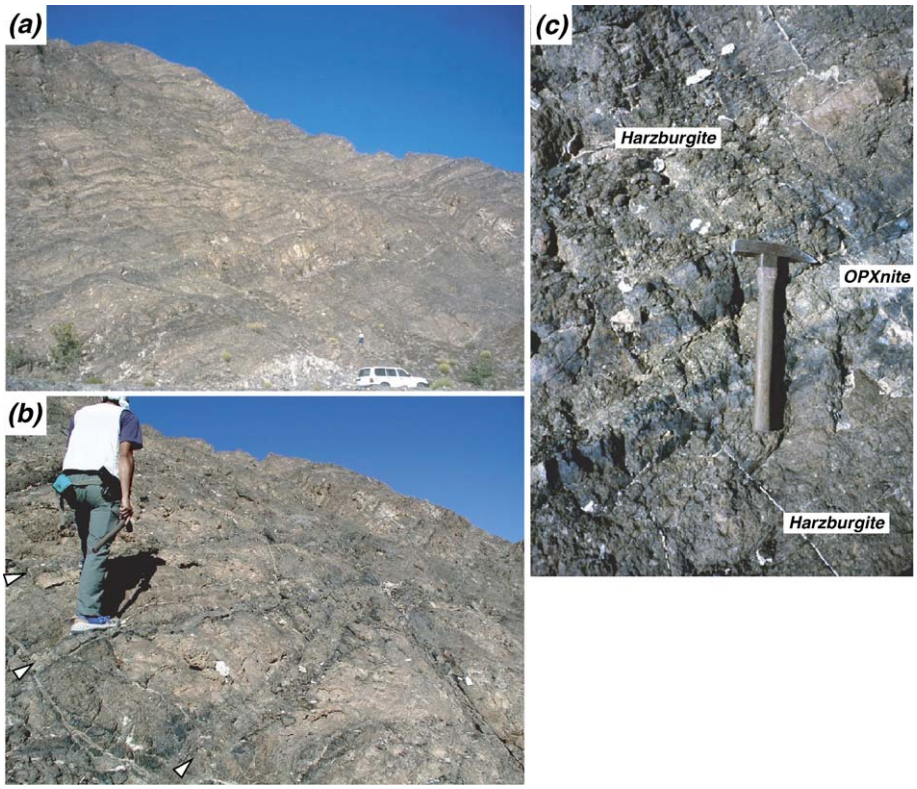

Fig. 2. (a) Panoramic view of the locality of the harzburgite–dunite–orthopyroxenite suit in the West Jizi block of the Oman ophiolite. The outcrop is the composed of dark and light colored bands. (b) A mode of occurrence of the harzburgite–dunite–orthopyroxenite suite in the Weste Jizi block in the Oman ophiolite. Arrows indicate the orthopyroxenite dikes. The dikes have black seams of alteration at the harzburgite contact. Each dike is subparallel and two dikes merged (center of photograph). (c) Orthopyroxenite dike in harzburgite. Harzburgite directly contacts with orthopyroxenite. The black seams are severely serpentinized harzburgite.

1986). In the study area the geological structure is complicated by many thrust faults, which form the boundaries between late intrusives and mantle peridotite (Fig. 1b).

The suite is mainly composed of harzburgite, as host rock, intruded by abundant orthopyroxenite dikes, and is similar in appearance to the banded unit described by Lippard et al. (1986) (Fig. 2a). The orthopyroxenite petrographically corresponds to a dike of "the pyroxenite family" classified by Python and Ceuleneer (2003). Several orthopyroxenite dikes can be observed as horizontally sub-parallel each other within host harzburgite, and some of them merged (Fig. 2b). Thin dunite layers (<10 cm in width) were rarely developed along boundaries between orthopyroxenite dike and host harzburgite. The host harzburgite is serpentinized to various degrees and no clear deformation feature can be observed. The orthopyroxenite dikes range from 5 cm to 30 cm in width and is often in direct contact with host harzburgite by severely altered boundary zones (Fig. 2c).

We examined two pairs of host harzburgite and orthopyroxenite dike; harzburgite–dunite–orthopyroxenite (samples P1DH and P1PYX) and harzburgite–orhthopyroxenite (P2D and P2PYX), and 1 pair of harzburgite–dunite (P3HARZ and P3DUN). Dunite (P1DH dunite) of the pair corresponds to olivine-rich part in a harzburgite sample (P1DH harzburgite). A harzburgite sample (Distal) collected far from orthopyroxenite dikes was also examined. We list modal compositions of the rocks in Table 1. Harzburgite is poor in clinopyroxene (<1.5 vol.%). The harzburgite exhibits weak deformed texture, such as protogranular or porphyroclastic textures; some olivine grains rarely have kink-band. Orthopyroxene and clinopyroxene grains are a few mm and smaller than 1 mm in diameter, respectively. One dunite sample (P3DUN) is relatively rich in euhedral spinel (3 vol.%). The orthopyroxenite is mainly composed of orthopyroxene (>95%) and contains small amount of clinopyroxene (<5 vol.%) and trace spinel (<0.9 vol.%), and is free of olivine. It has equigranular texture and is almost free from deformation. Clinopyroxene is interstitial to orthopyroxene and is sometimes altered or replaced by tremolite and fine magnetite. Orthopyroxene ranges from 1 to 5 mm while clinopyroxene is smaller than 1 mm in diameter. Euhedral or subhedral spinel (<0.5 mm in diameter) is interstitial to or included in orthopyroxene grains.

Table 1
Modal compositions of the primary minerals in harzburgite, dunite and orthopyroxenite

Sample	Olivine (%)	opx (%)	cpx (%)	Spinel (%)	cpx/pyx
Harzburgite–Dunite					
Harzburgite					
Distal	81.1	16.5	1.8	0.6	0.09
P1 DH	82.9	15.8	0.3	1.2	0.01
P2D[a]	77.8	21.2	–	0.9	–
P3Harz	76.0	21.3	1.4	1.2	0.06
Dunite					
P3Dun	96.1	0.9	–	3.0	–
Orthopyroxenite					
P1PYX	–	97.8	2.1	0.1	0.02
P2PYX	–	95.5	3.5	0.9	0.04

The composition was determined by point-counting.
Altered minerals were recalculated for primary minerals.
[a] Totally altered olivine and pyroxenes.

4. Mineral chemistry

4.1. Analytical method

Major-element analysis of minerals was carried out with JEOL super probe (JXA-8800) at Center for Cooperative Research of Kanazawa University. We adopted an acceleration voltage of 20 kV, a specimen current of 20 nA and a beam diameter of 3 μm. The data were corrected using a ZAF program (Bence and Albee, 1968). Trace element (Ti, Sr, Y, Zr and rare earth element (REE)) concentrations in clinopyroxene were determined by a laser ablation (193 nm ArF excimer: MicroLas GeoLas Q-plus)-inductively coupled plasma mass spectrometry (Agilent 7500S) (LA–ICP–MS) at the Incubation Business Laboratory Center of Kanazawa University (Ishida et al., 2004). See Morishita et al. (2004) for analytical details and quality of data. Each analysis was performed by ablating 50 μm diameter spots for clinopyroxene at 5 Hz with energy density of 8 J/cm^2 per pulse. Signal integration times were 50 s for a gas background interval and 50 s for an ablation interval. The NIST SRM 612 glass was used as the primary calibration standard and was analyzed at the beginning of each batch of <3–4 unknowns, with a linear drift correction applied between each calibration. The element concentration of NIST SRM 612 for the calibration is selected from the preferred values of Pearce et al. (1997). Data reduction was facilitated using Si as internal standards for clinopyroxene, based on SiO_2 contents obtained by EPMA analysis, following a protocol essentially identical to that outlined by Longerich et al. (1996). The accuracy of measurements estimated from analyses of reference material (NIST SRM 614) is better than 4% in relative standard deviation for all elements.

4.2. Results

Major element compositions of minerals and trace element concentrations of clinopyroxene are listed in Tables 2 and 3, respectively. Forsterite content (Fo) of olivine varies from 89.9 to 91.3 in harzburgite and dunite (Fig. 3). NiO content of olivine ranges from 0.28 to 0.41 wt.% and is dominantly higher than 0.35 wt.%. Spinels in all rocks are chromian spinel with high Cr# (=0.624–0.764) and low TiO_2 content (<0.18 wt.%) (Fig. 4). Spinel in dunite is systematically higher in Cr# and lower in Mg# [=Mg/(Mg+Fe^{2+}) atomic ratio] than that in harzburgite, and each orthopyroxenite sample is slightly different in Cr# and Mg# of spinel (Fig. 4). For the relationship between the Fo content of olivine and Cr# of spinel, harzburgite and dunite fall into the olivine–spinel mantle array (OSMA), a residual trend of spinel peridotite (Arai, 1987, 1994) (Fig. 3). The Mg# varies from 0.904 to 0.917 in orthopyroxene and varies from 0.934 to 0.942 in clinopyroxene (Fig. 5). Al_2O_3 contents of orthopyroxene and clinopyroxene range from 0.73 to 1.14 wt.% and from 0.92 to 1.49 wt.%, respectively. The Al_2O_3 content and Mg# of orthopyroxene are higher in harzburgite than in dunite. Orthopyroxenite falls into an area between dunite and harzburgite in terms of Mg#–Al_2O_3 relationship (Fig. 5). Na_2O content of clinopyroxene is very low (<0.2 wt.%). Two-pyroxene thermometry (Wells, 1977) indicates that the equilibrium temperature is from 926 °C to 1045 °C and 987 °C on average.

Clinopyroxene in harzburgite and orthopyroxenite is characterized by light REE (LREE)-depleted patterns [$(Ce/Yb)_{N(=\text{chondrite-normalized value})}$=0.008–0.12] (Fig. 6). The clinopyroxenes have very low heavy REE (HREE) concentrations [e.g., $(Yb)_N \leq 1$], and some trace element patterns display positive Sr anomaly. The HREE concentrations of clinopyroxene are lower in the harzburgites than in abyssal peridotite and similar to those in the most depleted harzburgite from the Oman ophiolite (Kelemen et al., 1995) and the forearc peridotite (Parkinson et al., 1992). The clinopyroxenes from the two harzburgite samples (Distal and P3HARZ) are significantly depleted in middle-REE (MREE) and LREE [e.g., $(Sm)_N$<0.22, $(Ce)_N$=0.010–0.039]. However, clinopyroxene shows flat pattern [$(La/Ce)_N$=0.77–0.96 and $(Ce/Nd)_N$=0.75–1.01] and high MREE and LREE concentrations [e.g., $(Sm)_N$< 0.19, $(Ce)_N$=0.068–0.098] relative to low HREE concentrations [e.g., $(Yb)_N$=0.75–0.83, $(Ce/Yb)_N$= 0.08–0.13] in one harzburgite sample (P1DH). Clinopyroxenes from the orthopyroxenite samples are similar in concentrations and patterns to the harzburgite (P1DH) with stronger positive Sr and negative Zr anomalies.

5. Discussion

5.1. Petrogenesis of the suite

The harzburgite–dunite–orthopyroxenite suite is characterized by the high Cr# (>0.65) of spinel. In the relationship between Cr# of spinel and Fo of olivine, the harzburgites fall within the OSMA (Arai, 1987, 1994) indicating the residual mantle peridotite (Fig. 3a). The Cr# of spinel is a good indicator of the degree of partial melting for the mantle-derived spinel peridotite (Dick and Bullen, 1984; Arai, 1994). It is higher in peridotite residue with a higher degree of melt extraction from partial melting, such as more deplete peridotite. The value is also useful to discriminate the tectonic setting of peridotite derived (Fig. 3b). For example, the Cr# of spinel in abyssal peridotites collected from mid-ocean ridges and fracture zones is less than 0.6. The value can be explained by partial melting and MORB magma extraction in the mid-ocean ridge stage (Kelemen et al., 1995). According to previous studies, the Cr# of spinel in the Oman harzburgite does not exceed 0.6 (e.g. Kelemen et al., 1995; Kadoshima, 2002; Takazawa et al., 2003) (Fig. 3a). However some studies recent pointed out the presence of highly deplete harzburgite with higher Cr# (>0.6) of spinel in several part of the Oman ophiolite (Matsukage et al., 2001; Le Mée et al., 2004; Kanke and Takazawa, 2005) (Fig. 4). Hellebrand et al. (2001) showed a negative relationships between Cr# of spinel and HREE concentration of clinopyroxene in abyssal peridotite (Fig. 7a). The harzburgites from the suite are concordant with the relationship; it is on the higher-Cr# extension of the abyssal peridotite trend (Cr#>0.6) in terms of Yb content of clinopyroxene (Fig. 7a). Therefore, the harzburgites are probably a residue of higher degree of partial melting. On the other hand, there is not good correlation between Cr# of spinel and LREE concentration of clinopyroxene due to variable LREE enrichments (e.g. Hellebrand et al., 2001) (Fig. 7b). In P1DH harzburgite, especially, LREE concentrations of clinopyroxene are quite high [e.g., $(Ce)_N \approx 0.08$] relative to highly depleted composition, such as high-Cr# of spinel (Cr#>0.7) and HREE concentrations of clinopyroxene [e.g., $(Yb)_N \approx 0.8$] (Fig. 7). The trace-element pattern of the clinopyroxene in P1DH harzburgite exhibits nearly flat in LREE (Fig. 6a). In order to explain the pattern of the highly depleted peridotite, the influx melting involving LREE-enriched melt/fluid is preferable to simple fractional melting or mantle–melt

Table 2
Major element compositions of olivine, spinel, orthopyroxene and clinopyroxene from the harzburgite (Harz)–dunite (Dun)–orthopyroxenite (OPXt) suite form the West Jizi block in the Oman ophiolite

Olivine

Sample	Distal		P1DH		P3Harz		P1DH		P3Dun	
	Harz	S.D.	Harz	S.D.	Harz	S.D.	Dun	S.D.	Dun	S.D.
SiO_2	40.86	0.19	40.44	0.16	40.42	0.41	40.14	0.22	40.63	0.09
FeO*	8.74	0.10	9.07	0.24	9.41	0.10	8.72	0.20	10.01	0.06
MnO	0.12	0.03	0.11	0.01	0.12	0.02	0.11	0.01	0.14	0.02
MgO	50.40	0.18	49.90	0.12	49.99	0.50	50.23	0.21	49.86	0.22
CaO	0.04	0.02	0.04	0.02	0.03	0.02	<0.02		<0.02	
NiO	0.37	0.02	0.33	0.01	0.36	0.02	0.39	0.01	0.28	0.02
Total	100.54		99.89		100.33		99.59		100.91	
Fo	91.1	0.1	90.7	0.2	90.4	0.2	91.1	0.2	89.9	0.0

Spinel

Sample	Distal		P1DH		P2D		P3Harz		P3Dun		P1DH		P1PYX		P2PYX	
	Harz	S.D.	Harz	S.D.	Harz	S.D.	Harz	S.D.	Dun	S.D.	Dun	S.D.	OPXt	S.D.	OPXt	S.D.
TiO_2	0.08	0.03	0.10	0.01	0.06	0.02	0.10	0.03	0.14	0.02	0.09	0.03	0.06	0.04	0.11	0.02
Al_2O_3	16.19	1.07	12.75	1.40	16.34	0.42	16.03	0.53	13.17	0.55	13.43	0.55	17.32	2.37	11.96	0.17
Cr_2O_3	51.60	1.25	53.57	0.52	51.59	0.32	50.64	0.44	51.43	0.44	54.34	0.62	49.56	3.64	57.19	0.56
Fe_2O_3	2.99	0.26	5.03	1.03	3.64	0.28	4.40	0.41	5.45	0.66	3.17	0.43	2.57	0.65	2.26	0.24
FeO	18.58	0.45	19.37	1.36	17.48	0.43	18.90	0.57	21.40	0.45	19.35	0.71	20.36	0.08	17.45	0.72
MnO	0.37	0.01	0.33	0.02	0.29	0.02	0.37	0.01	0.42	0.01	0.32	0.04	0.35	0.01	0.36	0.02
MgO	10.48	0.23	9.72	1.13	11.30	0.22	10.35	0.41	8.31	0.39	9.74	0.53	9.27	0.14	10.77	0.56
NiO	0.05	0.01	0.06	0.02	0.05	0.01	0.05	0.01	0.05	0.01	0.05	0.01	0.03	0.02	0.05	0.01
Total	100.34		100.92		100.73		100.84		100.37		100.49		99.52		100.13	
Mg#	0.501	0.011	0.472	0.046	0.535	0.011	0.494	0.017	0.409	0.016	0.473	0.023	0.448	0.005	0.524	0.023
Cr#	0.681	0.020	0.739	0.020	0.679	0.007	0.679	0.008	0.724	0.007	0.731	0.010	0.657	0.047	0.762	0.001
Cr/R^{3+}	0.657	0.017	0.693	0.011	0.650	0.005	0.643	0.006	0.675	0.002	0.702	0.008	0.637	0.051	0.741	0.002
Al/R^{3+}	0.307	0.020	0.245	0.023	0.307	0.007	0.304	0.009	0.257	0.009	0.259	0.010	0.332	0.043	0.231	0.002
Fe^{3+}/R^{3+}	0.036	0.003	0.062	0.014	0.044	0.003	0.053	0.005	0.068	0.009	0.039	0.005	0.031	0.008	0.028	0.003
Fe^{3+}/Fet	0.127	0.011	0.188	0.021	0.158	0.012	0.173	0.016	0.186	0.019	0.128	0.015	0.102	0.023	0.104	0.008

Orthopyroxene

Sample	Distal		P1DH		P3Harz		P3Dun		P1PYX		P2PYX	
	Harz	S.D.	Harz	S.D.	Harz	S.D.	Dun	S.D.	OPXt	S.D.	OPXt	S.D.
SiO_2	57.95	0.82	57.85	0.44	57.93	0.24	58.03	0.22	57.57	0.28	57.92	0.22
TiO_2	<0.05		<0.05		<0.05		<0.05		<0.05		<0.05	
Al_2O_3	1.05	0.04	0.93	0.00	1.10	0.05	0.81	0.12	0.93	0.11	0.89	0.03
Cr_2O_3	0.46	0.04	0.43	0.02	0.42	0.03	0.34	0.03	0.41	0.05	0.48	0.03
FeO*	5.67	0.07	5.95	0.11	6.08	0.05	6.48	0.01	5.90	0.31	6.19	0.14
MnO	0.14	0.02	0.11	0.00	0.15	0.02	0.17	0.00	0.14	0.01	0.17	0.02
MgO	34.77	0.27	34.65	0.33	34.53	0.12	34.59	0.34	34.02	1.31	34.01	0.72
CaO	1.24	0.32	1.10	0.12	1.09	0.15	0.65	0.17	1.93	1.67	1.61	0.72
Na_2O	<0.03		<0.03		<0.03		<0.03		<0.03		<0.03	
K_2O	<0.02		<0.02		<0.02		<0.02		<0.02		<0.02	
Total	101.29		101.01		101.29		101.07		100.90		101.26	
Mg#	0.916	0.001	0.912	0.002	0.910	0.001	0.905	0.001	0.911	0.002	0.907	0.001
Cr#	0.226	0.014	0.234	0.008	0.203	0.009	0.218	0.009	0.230	0.014	0.265	0.008

Table 2 (*continued*)

Clinopyroxene										
Sample	Distal		P1DH		P3Harz		P1PYX		P2PYX	
	Harz	S.D.	Harz	S.D.	Harz	S.D.	OPXt	S.D.	OPXt	S.D.
SiO_2	54.85	0.32	54.97	0.31	54.88	0.10	54.48	0.34	54.91	0.43
TiO_2	<0.05		<0.05		<0.05		<0.05		<0.05	
Al_2O_3	1.14	0.10	1.01	0.06	1.36	0.09	1.25	0.15	1.02	0.04
Cr_2O_3	0.66	0.07	0.58	0.08	0.72	0.07	0.67	0.07	0.79	0.04
FeO*	2.02	0.08	2.10	0.05	2.15	0.14	2.03	0.03	2.24	0.26
MnO	0.08	0.02	0.09	0.01	0.11	0.01	0.06	0.01	0.08	0.01
MgO	18.15	0.53	17.95	0.25	17.94	0.14	17.78	0.20	18.01	0.30
CaO	23.00	0.75	23.77	0.25	22.76	0.55	23.50	0.12	22.22	0.76
Na_2O	0.09	0.03	0.13	0.00	0.09	0.01	0.11	0.02	0.15	0.02
K_2O	<0.02		<0.02		<0.02		<0.02		<0.02	
Total	99.99		100.60		100.02		99.87		99.42	
Mg#	0.941	0.001	0.938	0.001	0.937	0.004	0.940	0.002	0.935	0.006
Cr#	0.281	0.002	0.277	0.016	0.261	0.006	0.264	0.006	0.343	0.016

Values on average of minerals in each sample. S.D.: standard deviation. Total iron as FeO* and Mg#=Mg/(Mg+Fe) atomic ratio and Cr#=Cr/(Cr+Al) atomic ratio.
FeO and Fe_2O_3 in spinel were calculated from stoichiometry and Mg#=Mg/(Mg+Fe^{2+}), R^{3+}=Cr+Al+Fe^{3+} and Fet=Fe^{2+}+Fe^{3+}.

interaction (e.g., Bizimis et al., 2000; Barth et al., 2003). The depleted composition suggests a re-melting process of peridotite that had once experienced partial melting. The fact that the LREE and Sr can be distributed to water (Tatsumi et al., 1986; Kogiso et al., 1997) implies that the flux contained H_2O and caused hydrous condition during melting. This situation and the high melting degree of the harzburgite support the re-melting with influx because the hydrous condition enhances the degree of partial melting of peridotite (e.g., Kushiro, 1969; Hirose and Kawamoto, 1995). Depleted harzburgite with high-Cr# spinel is most probably formed as a residue of partial melting assisted by H_2O-rich influx in the upper mantle (e.g., Hirose and Kawamoto, 1995; Matsukage and Kubo, 2003). This may explain the low-Fo olivine relative to high-Cr# spinel in harzburgite (Fig. 3a). Addition of Fe-rich fluid/melt could produce the harzburgite with relatively low-Fo olivine and high-Cr# spinel (Matsukage et al., 2001). The dunite plots at the extension of harzburgite in the Fo (olivine)–Cr# (spinel) space, implying the dunite was an end product of the influx melting.

Mode of occurrences of the orthopyroxenite in the suite, such as intrusive dike-like morphology and sharp boundary with the host harzburgite, suggests that the orthopyroxenite is probably a product of crystal fractionation during melt migration in upper mantle. The H_2O-rich influx melting of a peridotite produced a melt that had a reaction relation with olivine to produce orthopyroxene (e.g., Kushiro, 1969). This melt produced olivine-free orthopyroxene cumulate (orthopyroxenite) on cooling with or without decompression. The melt was genetically related to the origin of host harzburgite mentioned above. The most depleted peridotite, such as P1DH harzburgite, is similar in geochemical signature to the orthopyroxenite. Therefore, P1DH harzburgite probably corresponds to residual material of the partial melt forming the orthopyroxenite. The partial melt was probably rich in Mg and Cr, and was a Si-rich magma primarily crystallizing orthopyroxene because H_2O assisted not only to enhance the melting degree but also to form the Si-rich melt upon partial melting of peridotite (e.g. Kushiro, 1972, 1974). The boninite magma is a primarily Si-rich melt in equilibrium with mantle harzburgite (e.g., Kuroda et al., 1978; Umino and Kushiro, 1989), and is a candidate for the melt involved. The high-Cr# character of spinel also suggests a linkage to boninite (Fig. 4). Type of the melt was estimated from the trace element concentrations of clinopyroxene. The equilibrium melt with orthopyroxenite and P1DH harzburgite were calculated using clinopyroxene/melt distribution coefficients by Sobolev et al. (1996) and assuming that the trace elements are completely distributed in clinopyroxene (Fig. 8). The calculated melt is similar in not only HREE concentrations and flat LREE pattern but also positive Sr and Zr anomalies to boninite rather than pattern of MORB (Fig. 8). Two-pyroxene geothermometry (Wells, 1977) indicates the equilibrium temperature around 1000 °C, which suggests that the clinopyroxene possibly coexist with the melt. However, the subsolidus origin can not be ruled out considering the low volume ratio of clinopyroxene to total pyroxenes (<10%, Table 1) and the two-

Table 3
Trace element and REE compositions (ppm) of clinopyroxene in harzburgite and orthopyroxenite from the West Jizi block in the Oman ophiolite

Sample	Harzburgite									Orthopyroxenite								DL	Kd
	Distal			P1DH			P3Harz[a]			P1PYX						P2OPX			
	A1	A2	I	A	C	E	A	E	G	D	E	F	Y	Z	W	C	J		
Ti	160	176	100	165	174	157	227	206	201	206	188	159	218	261	195	207	219	1.9	0.229
Sr	0.553	0.598	0.303	0.529	1.079	1.273	1.159	0.529	0.572	1.691	2.332	5.254	1.878	1.843	1.975	1.824	2.685	0.034	0.082
Y	1.488	1.740	0.622	1.091	1.064	1.107	1.450	1.336	1.241	1.135	1.007	0.789	1.305	1.467	1.097	1.551	1.227	0.012	0.245
Zr	0.366	0.420	0.136	0.401	0.420	0.338	0.154	0.177	0.182	0.209	0.190	0.149	0.261	0.295	0.201	0.291	0.230	0.022	0.046
La	–	–	–	0.014	0.022	0.013	–	–	–	–	–	–	–	–	–	–	0.018	0.010	0.032
Ce	0.019	0.024	0.009	0.041	0.060	0.044	0.010	0.005	0.011	0.028	0.029	0.022	0.035	0.038	0.031	0.027	0.058	0.007	0.057
Pr	–	–	–	0.008	0.010	–	–	–	–	–	–	–	–	0.006	–	–	–	0.007	
Nd	–	–	–	0.042	0.046	0.042	–	0.021	0.028	–	0.033	–	0.041	0.038	–	0.045	0.057	0.029	0.129
Sm	–	–	–	0.029	–	–	–	0.034	–	0.030	–	–	–	–	–	–	–	0.029	0.211
Eu	–	–	–	0.014	0.017	–	0.015	–	0.015	–	0.013	–	–	0.016	–	0.024	0.023	0.011	
Gd	0.079	0.112	0.028	0.069	0.069	0.067	0.067	0.079	0.080	–	0.064	–	0.092	0.092	0.071	0.125	0.127	0.030	
Tb	0.024	0.023	0.010	0.019	0.020	0.018	0.024	0.024	0.020	0.019	0.012	0.014	0.021	0.027	0.019	0.028	0.025	0.010	
Dy	0.235	0.292	0.082	0.160	0.164	0.173	0.237	0.212	0.194	0.157	0.168	0.117	0.21	0.236	0.165	0.275	0.231	0.035	0.256
Ho	0.066	0.097	0.024	0.040	0.035	0.037	0.059	0.057	0.053	0.041	0.039	0.031	0.054	0.063	0.048	0.055	0.058	0.013	
Er	0.201	0.277	0.072	0.118	0.126	0.138	0.227	0.190	0.178	0.147	0.132	0.097	0.162	0.175	0.139	0.199	0.167	0.019	0.259
Tm	0.037	0.043	0.009	0.019	0.024	0.020	0.034	0.032	0.031	0.021	0.019	0.013	0.027	0.028	0.017	0.031	0.025	0.011	
Yb	0.237	0.301	0.086	0.141	0.128	0.139	0.214	0.183	0.186	0.139	0.134	0.113	0.169	0.203	0.159	0.194	0.167	0.028	0.214
Lu	0.034	0.046	0.015	0.021	0.019	0.028	0.035	0.033	0.031	0.023	0.022	0.015	0.025	0.031	0.030	0.025	0.020	0.012	

–: below detection limit.
DL: detection limit except for P3Harz.
Kd: clinopyroxene/melt distribution coefficient (Sobolev et al., 1996).
[a] P3Harz measured under higher sensitivity condition for MLREE, and lower detection limit (La: 0.005, Ce: 0.003, Pr: 0.004, Nd: 0.020).

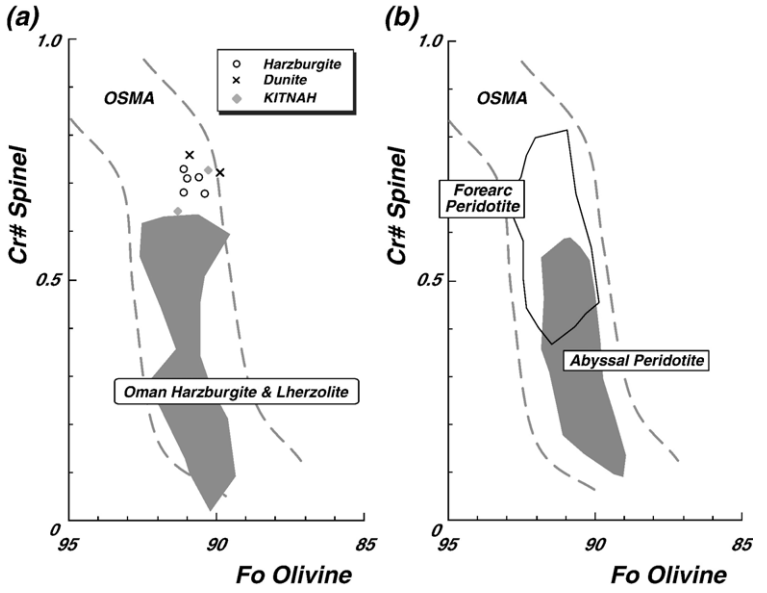

Fig. 3. (a) Compositional relationship between Fo content of olivine and Cr# [=Cr/(Cr+Al) atomic ratio] of spinel in the harzburgite and dunite from the suite in the West Jizi block of the Oman ophiolite. OSMA (olivine–spinel mantle array; Arai, 1987, 1994) is a spinel peridotite restite trend. Range of Oman harzburgite and lherzolite are from Kadoshima (2002) and Takazawa et al. (2003). "KITNAH" which is mylonitic harzburgite and dunite from the Wadi Kitnah area is shown for comparison. (b) Ranges of the same relationship for abyssal peridotite (Dick and Bullen, 1984; Arai, 1994) and forearc peridotite (Bloomer and Hawkins, 1983; Bloomer and Fisher, 1987; Ishii et al., 1992; Parkinson and Pearce, 1998).

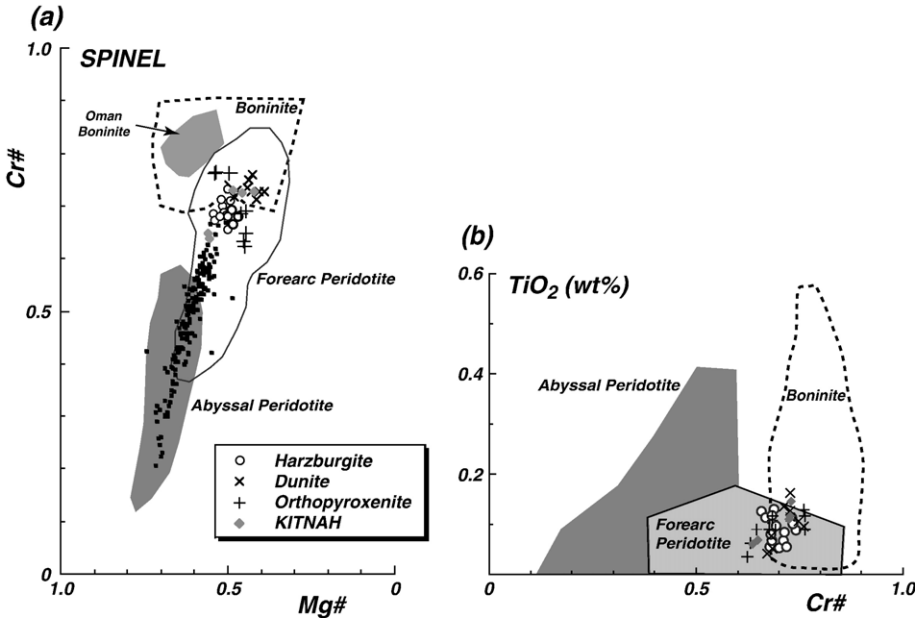

Fig. 4. Compositional variations of spinel in the harzburgite–dunite–orthopyroxenite suite from the West Jizi block of the Oman ophiolite. (a) Relationship between Mg# [=Mg/(Mg+Fe^{2+}) atomic ratio] and Cr# [=Cr/(Cr+Al) atomic ratio]. Black dots are Oman harzburgite, data from Le Mée et al. (2004). (b) Relationship between Cr# and TiO_2 content. KITNAH: see Fig. 3. For ranges of abyssal peridotite and forearc peridotite, see references in Fig. 3. General boninite field is from Umino (1986), van der Laan et al. (1992), Cameron (1985) and Sobolev and Danyushevsky (1994). The Oman boninite field is from Ishikawa et al. (2002).

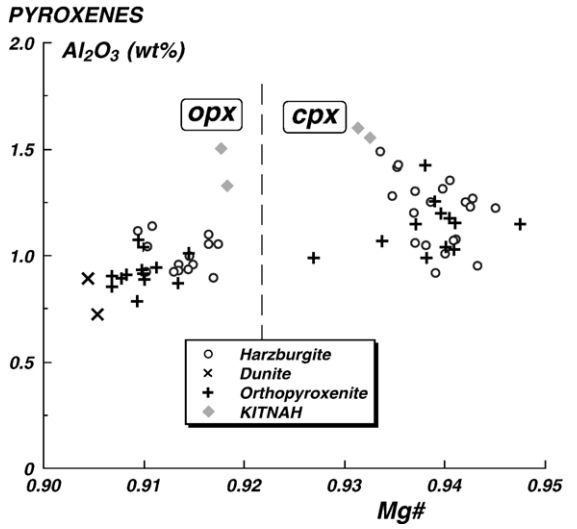

Fig. 5. Relationship between Mg# (=Mg/(Mg+Fe)) and Al_2O_3 content of orthopyroxene and clinopyroxene in the harzburgite–dunite–orthopyroxenite suite from the West Jizi block of the Oman ophiolite. KITNAH: see Fig. 3.

pyroxene solvus (e.g., Mori and Green, 1976; Lindsley and Dixon, 1976). This can explain the discrepancy that the calculated melt is slightly lower in MREE concentrations (Nd and Sm) than boninite (Fig. 8). The clinopyroxene has been in equilibrium not directly with melt at high temperatures but with orthopyroxene at subsolidus temperatures. If the temperature dependence of clinopyroxene/melt partition coefficient is not so different for one trace element from another, the "hypothetical melt" in equilibrium with the subsolidus clinopyroxene may mimic the "real melt" in trace-element characteristics. The relatively high HREE contents of the calculated melt (Fig. 8) may inherit from orthopyroxene which favors HREE (e.g., Neumann et al., 2002).

5.2. Tectonic implications from the suite in the Oman ophiolite

The origin of the host harzburgite and orthopyroxenite suggests that the suite was formed within the supra-subduction zone mantle. The subducted slab is good account for petrogenesis for provided the LREE-enriched material with H_2O to the overlying mantle. Python and Ceuleneer (2003), however, discussed that their "depleted suite" including orthopyroxenite can be formed from the melt at the mid-ocean ridge stage, evidenced from reports of depleted melts in the setting (Ross and Elthon, 1993; Sobolev and Shimizu, 1993). In our study, we showed not only cumulative rocks from the depleted melt but also residual material (harzburgite). No depleted harzburgite with high-Cr# spinel, exceeding 0.6, has been reported from mid-ocean ridge setting (Fig. 3b), although critically depleted melts indicating possibility of high degree of melting were reported (e.g.,

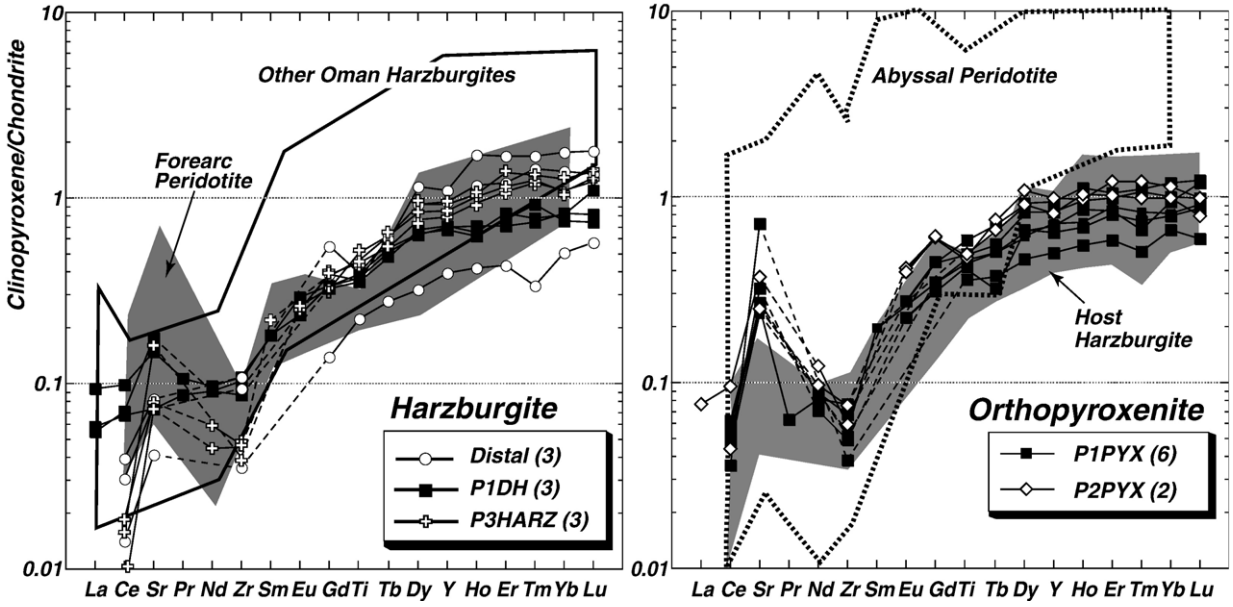

Fig. 6. Chondrite-normalized Ti, Sr, Y, Zr and REE concentrations in clinopyroxene in harzburgite (a) and orthopyroxenite (b) from the suite in the West Jizi block of the Oman ophiolite. Number of analyzed clinopyroxene given in parentheses. Other Oman harzburgites are from Kelemen et al. (1995). The range of forearc peridotite is from Parkinson et al. (1992). The range of abyssal peridotites is from Johnson et al. (1990), Johnson and Dick (1992) and Hellebrand et al. (2002). Chondrite data are from Sun and McDonough (1989).

Nannotte et al., 2005). On the other hand, highly depleted peridotites collected from the landward flank of trench and serpentine seamounts in the western Pacific were derived from the fore-arc part of supra-subduction zone mantle (e.g., Bloomer and Hawkins, 1983; Ishii et al., 1992; Parkinson et al., 1992). They are similar in petrological features, especially the high Cr# of spinel and trace-element pattern of clinopyroxene, to the host harzburgite in the suite (Figs. 3 and 6). The boninite magma activity has been actually restricted within the supra-subduction zone (Pearce et al., 1992; Taylor et al., 1994). The boninite magma-related material within mantle sequence, such as pyroxenite and residual peridotite, even suggests that the ophiolitic complex has originated the supra-subduction zone setting (e.g. Edwards, 1995; Varfalvy et al., 1996, 1997; Suhr and Edwards, 2000). Although the harzburgite similar in mineral composition to abyssal one is prevalent within the Oman ophiolite mantle (e.g., Boudier and Coleman, 1981; Kelemen et al., 1995; Kadoshima, 2002; Takazawa et al., 2003), the highly depleted harzburgite associated with refractory orthopyroxenite and dunite that recorded arc magmatism is locally present. The studied suite is a deep-seated equivalent to volcanics of arc signature, especially boninite (Ishikawa et al., 2002). Igneous rocks of arc signature were added to oceanic lithosphere on obduction, which was coupled with subduction (see Arai, 1995; Ishikawa et al., 2002; Arai et al., 2004). Such sort of modification may be indispensable to the slice of oceanic lithosphere that had appeared on-land as ophiolite.

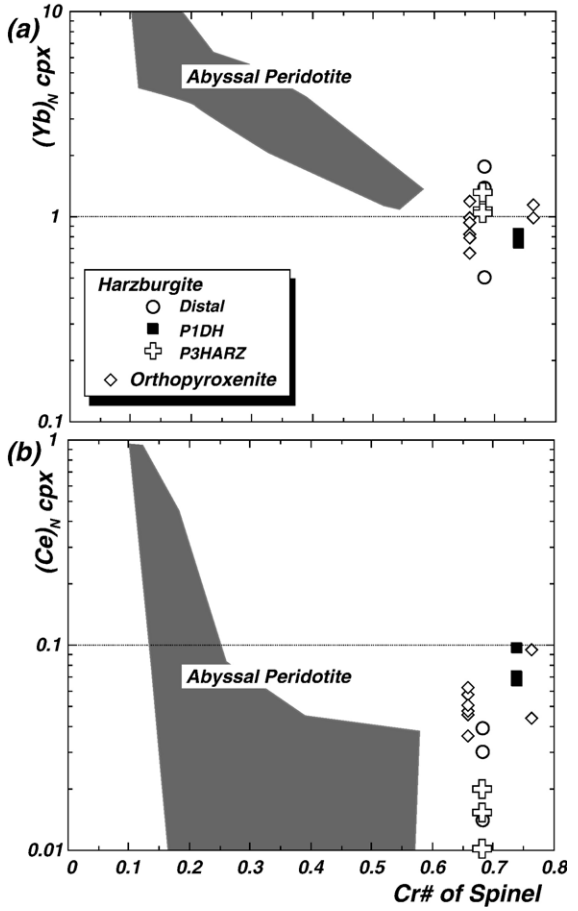

Fig. 7. Compositional relationships between Cr# (=Cr/(Cr+Al)) of spinel and chondrite-normalized trace element concentrations of clinopyroxene in harzburgite and orthopyroxenite from the suite in the West Jizi block of the Oman ophiolite. Chondrite data are from Sun and McDonough (1989). (a) Cr# of spinel vs. $(Yb)_{N(=\text{chondrite-normalized value})}$. (b) Cr# vs. $(Ce)_N$. Abyssal peridotite field is from Hellebrand et al. (2001).

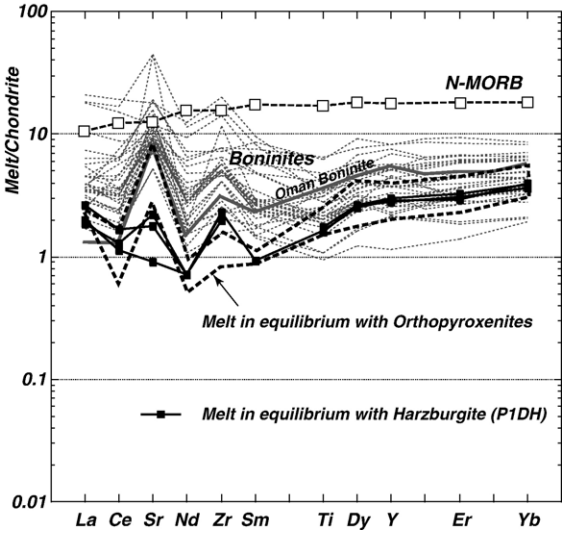

Fig. 8. Chondrite-normalized trace element concentrations for melt in equilibrium with orthopyroxenites and harzburgite (P1DH). The melt compositions were calculated by using clinopyroxene/melt distribution coefficients from Sobolev et al. (1996) (Table 3) and by assuming that the trace elements are completely distributed in clinopyroxene. General boninites (gray broken lines) are from Cameron et al. (1983), Cameron (1985), and Taylor et al. (1994) and the Oman boninite (gray bold line) is from Ishikawa et al. (2005). N-MORB and chondrite data are from Sun and McDonough (1989).

6. Conclusions

1. We found a refractory suite of harzburgite–orthopyroxenite–dunite from the northern Oman ophiolite. They have refractory mineral chemistry and lithology: the harzburgite and dunite are of residual origin of high-degree partial melting assisted by H_2O-rich influx, and the orthopyroxenite was a cumulate from the partial melt.

2. The melt in equilibrium with their clinopyroxene was similar in trace-element characteristics to a boninite. Deep-seated boninitic magmatism could have produced the refractory suite of harzburgite–orthopyroxenite–dunite.
3. The harzburgite–orthopyroxenite–dunite suite has recorded a supra-subduction zone setting within the mantle section of the Oman ophiolite. The igneous rocks of arc signature were added to a slice of oceanic lithosphere upon its obduction as an ophiolite.

Acknowledgements

We are grateful to J. Uesugi, S. Miyashita and Ministry of Commerce and Industry of Oman for their help for field work in the Oman ophiolite. A. Ishiwatari and T. Morishita are thanked for constructive comments. Y. Shimizu, K. Tazaki and Y. Ishida are acknowledged for assistance with the electron microprobe and LA–ICP–MS. Manuscript was greatly improved by constructive comments of two anonymous reviewers.

References

Alabaster, T., Pearce, J.A., Malpas, J., 1982. The volcanic stratigraphy and petrogenesis of the Oman ophiolite complex. Contributions to Mineralogy and Petrology 81, 168–183.

Arai, S., 1987. An estimation of the least depleted spinel peridotite on the basis of olivine–spinel mantle array. Neues Jahrbuch für Mineralogie Monatshefte 8, 347–354.

Arai, S., 1994. Characterization of spinel peridotites by olivine–spinel compositional relationships: review and interpretation. Chemical Geology 113, 191–204.

Arai, S., 1995. Oceanic lithosphere and ophiolites; their similarities and differences. Journal of Geography 104 (3), 361J–380J.

Arai, S., Uesugi, J., Ahmed, A.H., 2004. Upper crustal podiform chromitite from the northern Oman ophiolite as the stratigraphically shallowest chromitite in ophiolite and its implication for Cr concentration. Contributions to Mineralogy and Petrology 147 (2), 145–154.

Barth, M.G., Manson, P.R.D., Davies, G.R., Dijkstra, A., Drury, M.R., 2003. Geochemistry of the Othris ophiolite, Greece: evidence for refertilization? Journal of Petrology 44, 1759–1785.

Batanova, V.G., Sobolev, A.V., 2000. Compositional heterogeneity in subduction-related mantle peridotites, Troodos massif, Cyprus. Geology 28, 55–58.

Bence, A.E., Albee, A.L., 1968. Empirical correction factors for the electron microanalysis of silicates and oxides. Journal of Geology 76, 382–403.

Bizimis, M., Salters, V.J.M., Bonatti, E., 2000. Trace and REE content of clinopyroxenes from supra-subduction zone peridotite. Implications for melting and enrichment processes in island arcs. Chemical Geology 165, 67–85.

Bloomer, S.H., Fisher, R.L., 1987. Petrology and geochemistry of igneous rocks from the Tonga Trench – a non-accreting plate boundary. Journal of Geology 95, 469–495.

Bloomer, S.H., Hawkins, J.W., 1983. Gabbroic and ultramafic rocks from the Mariana trench: an island arc ophiolite. In: Hayes, D.E. (Ed.), The Tectonics and Geologic Evolution of Southeast Asian Seas and Islands: Part II. AGU Geophysical Monograph, vol. 23. American Geophysical Union, Washington, pp. 294–317.

Boudier, F., Coleman, R.G., 1981. Cross section through the peridotite in the Samail ophiolite, southeastern Oman. Journal of Geophysical Research 86, 2573–2593.

Cameron, W.E., 1985. Petrology and origin of primitive lavas from Troodos ophiolite, Cyprus. Contributions to Mineralogy and Petrology 89, 239–255.

Cameron, W.E., McCulloch, M.T., Walker, D.A., 1983. Boninite petrogenesis: chemical and Nd–Sr isotopic constraints. Earth and Planetary Science Letters 65, 75–89.

Dick, H.J.B., Bullen, T., 1984. Chromian spinel as a petrogenetic indicator in abyssal and alpine-type peridotites and spatially associated lavas. Contributions to Mineralogy and Petrology 86, 54–76.

Edwards, S.J., 1995. Boninitic and tholeiitic dykes in the Lewis Hills mantle section of the Bay of Islands ophiolite: implications for magmatism adjacent to a fracture zone in a back-arc spreading environment. Canadian Journal of Earth Sciences 32, 2128–2146.

Godard, M., Jousselin, D., Bodinier, J.-L., 2000. Relationships between geochemistry and structure beneath a palaeo-spreading centre: a study of the mantle section in the Oman ophiolite. Earth and Planetary Science Letters 180, 133–148.

Gregory, R.T., 1984. Melt percolation beneath a spreading ridge: evidence from the Semail peridotite, Oman. In: Gass, I.G., Lippard, S.J., Shelton, A.W. (Eds.), Ophiolite and Oceanic Lithosphere. Geological Society Special Publication, vol. 13. Geological Society, London, pp. 55–62.

Hellebrand, E., Snow, J.E., Dick, H.J.B., Hofman, A.W., 2001. Coupled major and trace elements as indicators of the extent of melting in mid-ocean-ridge peridotites. Nature 410, 677–681.

Hellebrand, E., Snow, J.E., Hoppe, P., Hofmann, A., 2002. Garnet-field melting and late-stage refertilization in 'residual' abyssal peridotites from the Central Indian Ridge. Journal of Petrology 43, 2305–2338.

Hirose, K., Kawamoto, T., 1995. Hydrous partial melting of lherzolite at 1 GPa: the effect of H_2O on the genesis of basaltic magmas. Earth and Planetary Science Letters 133, 463–473.

Ishida, Y., Morishita, T., Arai, S., Shirasaka, M., 2004. Simultaneous in-situ multi-element analysis of minerals on thin section using LA–ICP–MS. The Science Reports of Kanazawa University, vol. 48, pp. 31–42.

Ishii, T., Robinson, P.T., Maekawa, H., Fiske, R., 1992. Petrological studies of peridotites from diapiric serpentinite seamounts in The Izu–Ogasawara–Mariana forearc, LEG125. In: Fryer, P., Pearce, J.A., Stokking, L.B. (Eds.), Proceedings of the Ocean Drilling Program. Scientific Results, vol. 125. Ocean Drilling Program, College Station, Texas, pp. 445–485.

Ishikawa, T., Nagahashi, K., Umino, S., 2002. Boninitic volcanism in the Oman ophiolite: implications for thermal condition during transition from spreading ridge to arc. Geology 30, 899–902.

Ishikawa, T., Fujisawa, S., Nagahashi, K., Masuda, T., 2005. Trace element characteristics of the fluid liberated from amphibolite–facies slab: inference from the metamorphic sole beneath the Oman ophiolite and implication for boninite genesis. Earth and Planetary Science Letters 240, 355–377.

Johnson, K.T.M., Dick, H.J.B., 1992. Open system melting and temporal and spatial variation of peridotite and basalt at the

Atlantis II Fracture Zone. Journal of Geophysical Research 97, 9219–9241.

Johnson, K.T.M., Dick, H.J.B., Shimizu, N., 1990. Melting in the oceanic upper mantle: an ion microprobe study of diopsides in abyssal peridotites. Journal of Geophysical Research 95, 2661–2678.

Kadoshima, K., 2002. Petrological characteristics of the mantle section of the northern Oman and Lizard ophiolites: an approach from in-situ rocks and detrital chromian spinel. PhD thesis, Kanazawa University. 107 pp.

Kanke, N., Takazawa, E., 2005. Distribution of ultra-depleted peridotites in the northern Fizh mantle section from the Oman ophiolite. Abstract for Japan Earth and Planetary Science Joint Meeting, pp. J004–J029.

Kelemen, P.B., Shimizu, N., Salters, V.J.M., 1995. Extraction of mid-ocean-ridge basalt from the upwelling mantle by focused flow of melt in dunite channels. Nature 375, 747–753.

Kogiso, T., Tatsumi, Y., Nakano, S., 1997. Trace element transport during dehydration processes in the subducted oceanic crust: 1. Experiments and implications for the origin of oceanic island basalts. Earth and Planetary Science Letters 148, 193–206.

Kuroda, N., Shiraki, K., Urano, H., 1978. Boninite as a possible calc–alkalic primary magma. Bulletin of Volcanology 41, 563–575.

Kushiro, I., 1969. The system forsterite–diopside–silica with and without water at high pressures. American Journal of Science 267-A, 269–294.

Kushiro, I., 1972. Effect of water on the composition of magmas formed at high pressures. Journal of Petrology 13, 311–334.

Kushiro, I., 1974. Melting of hydrous upper mantle and possible generation of andesitic magma: an approach from synthetic systems. Earth and Planetary Science Letters 22, 294–299.

Le Mée, L., Girardeau, J., Monnier, C., 2004. Mantle segmentation along the Oman ophiolite fossil mid-ocean ridge. Nature 432, 167–172.

Le Métour, J., Béchennec, F., Chévremont, P., Roger, J., Wyns, R., 1992. Geological map of Buraymi, Sheet NG 40-14, Scale 1:250000, with explanatory notes. Directorate General of Minerals Ministry of Petroleum and Minerals, Sultanate of Oman.

Lindsley, D.H., Dixon, S.A., 1976. Diopside–enstatite equilibria at 850 °C to 1400 °C, 5 to 35 kb. American Journal of Science 276, 1285–1301.

Lippard, S.J., Shelton, A.W., Gass, I.G., 1986. The Ophiolite of Northern Oman. Geological Society Memoir, vol. 11. Geological Society by Blackwell Scientific Publications, London. 178 pp.

Longerich, H.P., Jackson, S.E., Gunther, D., 1996. Laser ablation inductively coupled plasma mass spectrometric transient signal data acquisition and analyte concentration calculation. Journal of Analytical Atomic Spectrometry 11, 899–904.

Matsukage, K., Kubo, K., 2003. Chromian spinel during melting experiments of dry peridotite (KLB-1) at 1.0–2.5 GPa. American Mineralogist 88, 1271–1278.

Matsukage, K., Arai, S., Abe, N., Yurimoto, H., 2001. Two contrasting melting styles of mantle peridotite in the northern Oman ophiolite: an indication of a switch of their tectonic setting. Research Report of JSPS Grants-in-Aid for Science Research, vol. 11691121, pp. 19–32.

Mori, T., Green, D.H., 1976. Subsolidus equilibria between pyroxenes in the CaO–MgO–SiO_2 system at high pressures and temperatures. American Mineralogist 61, 616–625.

Morishita, T., Ishida, Y., Arai, S., Shirasaka, M., 2004. Determination of multiple trace element compositions in thin (<30 μm) layers of NIST SRM 614 and 616 using laser ablation–inductively coupled plasma–mass spectrometry. Geostandards and Geoanalytical Research 29, 107–122.

Nannotte, P., Ceuleneer, G., Benoit, M., 2005. Genesis of andesitic–boninitic magmas at mid-ocean ridges by melting of hydrated peridotites: geochemical evidence from DSDP Site 334 gabbronorites. Earth and Planetary Science Letters 236, 632–653.

Neumann, E.R., Wullff-Pendersen, E., Pearson, N.J., Spencer, E.A., 2002. Mantle xenoliths from Tenerife (Canary Islands): evidence for reactions between mantle peridotites and silicic carbonatite melts inducing Ca metasomatism. Journal of Petrology 43, 825–857.

Nicolas, A., 1989. Structures of Ophiolites and Dynamics of Oceanic Crustal Analogues. Kluwer Academic Publication, Dordrecht. 367 pp.

Parkinson, I.J., Pearce, J.A., 1998. Peridotites from the Izu–Bonin–Mariana forearc (ODP Leg 125): evidence for mantle melting and melt–mantle interaction in a supra-subduction zone setting. Journal of Petrology 39, 1577–1618.

Parkinson, I.J., Pearce, J.A., Thirlwall, M.F., Johnson, K.T.M., Ingram, G., 1992. Trace element geochemistry of peridotites from the Izu–Bonin–Mariana forearc. In: Fryer, P., Pearce, J.A., Stokking, L.B. (Eds.), Proceedings of the Ocean Drilling Program, Scientific Results, vol. 125. Ocean Drilling Program, College Station, TX, pp. 487–506.

Pearce, J.A., van der Laan, S.R., Arculus, R.J., Murton, B.J., Ishii, T., Peate, D.W., Parkinson, I.J., 1992. Boninite and harzburgite from LEG 125 (Bonin–Mriana Forearc): a case study of magma genesis during the initial stages of subduction. In: Fryer, P., Pearce, J.A., Stokking, L.B. (Eds.), Proceedings of the Ocean Drilling Program, Scientific Results, vol. 125. Ocean Drilling Program, College Station, TX, pp. 623–657.

Pearce, N.J.G., Perkins, W.T., Westgate, J.A., Gorton, M.P., Jackson, S.E., Neal, C.R., Chenery, S.P., 1997. A compilation of new and published major and trace element data for NIST SRM 610 and NIST SRM 612 glass reference materials. Geostandards Newsletter 21, 115–144.

Python, M., Ceuleneer, G., 2003. Nature and distribution of dykes and related melt migration structures in the mantle section of the Oman ophiolite. Geochemistry Geophysics Geosystems 4 (7).

Ross, K., Elthon, D., 1993. Cumulates from strongly depleted mid-ocean ridge basalts. Nature 365, 826–829.

Sobolev, A.V., Danyushevsky, L.V., 1994. Petrology and geochemistry of boninites form the north termination of the Tonga trench: constraints on the generation conditions of primary high-Ca boninite magmas. Journal of Petrology 35, 1183–1211.

Sobolev, A.V., Shimizu, N., 1993. Ultra-depleted primary melt included in olivine from the Mid-Atlantic Ridge. Nature 363, 151–154.

Sobolev, A.V., Migdisov, A.A., Portnyagin, M.V., 1996. Incompatible element partitioning between clinopyroxene and basalt liquid revealed by the study of melt inclusions in minerals from Troodos lavas, Cyprus. Petrology 4, 307–317.

Suhr, G., Edwards, S.J., 2000. Contrasting mantle sequences exposed in the Lewis Hills massif: evidence for the early, arc-related history of the Bay of Islands ophiolite. In: Dilek, Y., Moores, E.M., Elthon, D., Nicolas, A. (Eds.), Ophiolites and Oceanic Crust: New Insights from Field Studies and the Oceanic Drilling Program. Special Paper-Geological Society of America, vol. 349. Geological Society of America, Boulder, CO, pp. 433–442.

Sun, S.S., McDonough, W.F., 1989. Chemical and isotopic systematics of oceanic basalts: implications for mantle composition and

processes. In: Saunders, A.D., Norry, M.J. (Eds.), Magmatism in the Ocean Basins. Geological Society Special Publication, vol. 42. Geological Society, London, pp. 313–345.

Takazawa, E., Okayasu, T., Satoh, K., 2003. Geochemistry and origin of the basal lherzolites from the northern Oman ophiolite (northern Fizh block). Geochemistry Geophysics Geosystems 4 (2).

Tatsumi, Y., Hamilton, D.L., Nesbitt, R.W., 1986. Chemical characteristics of fluid phase released from a subducted lithosphere and origin of arc magmas: evidence from high-pressure experiments and natural rocks. Journal of Volcanology and Geothermal Research 29, 293–303.

Taylor, R.N., Nesbitt, R.W., Vidal, P., Harmon, R.S., Auvray, B., Croudace, I.W., 1994. Mineralogy, chemistry, and genesis of the boninite series volcanics, Chichijima, Bonin Islands, Japan. Journal of Petrology 35, 577–617.

Tilton, G.R., Hopson, C.A., Wright, J.E., 1981. Uranium–lead isotopic ages of the Samail ophiolite, Oman, with applications to Tethyan ocean ridge tectonics. Journal of Geophysical Research 86, 2763–2775.

Umino, S., 1986. Magma mixing in boninite sequence of Chichijima, Bonin island. Journal of Volcanology and Geothermal Research 29, 125–157.

Umino, S., Kushiro, I., 1989. Experimental studies on boninite petrogenesis. In: Crowford, A.J. (Ed.), Boninites and Related Rocks. Unwin Hyman, London, pp. 89–111.

van der Laan, S.R., Arculus, R.J., Pearce, J.A., Murton, J.B., 1992. Petrography, mineral chemistry, and phase relations of the basement boninite series of Site 786, Izu–Bonin forearc. In: Fryer, P., Pearce, J.A., Stokking, L.B. (Eds.), Proceedings of the Ocean Drilling Program, Scientific Results, vol. 125. Ocean Drilling Program, College station, TX, pp. 171–202.

Varfalvy, V., Hebert, R., Bedard, J.H., 1996. Interactions between melt and upper-mantle peridotites in the North Arm Mountain massif, Bay of islands ophiolite, Newfoundland, Canada: implications for the genesis of boninitic and related magmas. Chemical Geology 129, 71–90.

Varfalvy, V., Hébert, R., Bédard, J.H., Lafléche, M.R., 1997. Petrology and geochemistry of pyroxenite dykes in upper mantle peridotite of the North Arm Mountain massif, Bay of Islands ophiolite, Newfoundland: implications for the genesis of boninitic and related magmas. Canadian Mineralogist 35, 543–570.

Wells, P.R.A., 1977. Pyroxene thermometry in simple and complex systems. Contributions to Mineralogy and Petrology 62, 129–139.